A lifetime of changing calls: North Atlantic right whales (*Eubalaena glacialis*) refine call production as they age

Authors: Holly Root-Gutteridge[a], Dana A. Cusano[a], Yu Shiu[b], Douglas P. Nowacek[c], Sofie M. Van Parijs[d], Susan E. Parks[a]

Author affiliations:

[a]Department of Biology, Syracuse University, New York

[b]Bioacoustics Research Program, Lab of Ornithology, Cornell University, Ithaca, New York

[c]Nicholas School of the Environment and Pratt School of Engineering, Duke University Marine Lab, Beaufort, North Carolina

[d]Northeast Fisheries Science Center, NOAA Fisheries, Woods Hole, Massachusetts

Orcid ID: http://orcid.org/0000-0001-9854-2948 (HRG), (SVJ) , (DAC), http://orcid.org/0000-0002-8137-1836 (DPN), http://orcid.org/0000-0001-6663-627X (SEP)

Corresponding author:

Holly Root-Gutteridge, 277 Life Sciences Building, Syracuse University, 107 College Place, Syracuse, NY 13244. Tel: +1 315 443 0194. Email: hollyrg@googlemail.com

Word count: 8,615, without bibliography

Morphology-controllable synthesis of highly ordered nanoporous diamond films

Qiang Wang[a], Jie Bai[a], Bing Dai[a], Lei Yang[a], Peng Wang[a], Zhenhuai Yang[a], Shuai Guo[a], Yumin Zhang[a], Jiecai Han[a], Jiaqi Zhu[a,b,*]

[a] Center for Composite Materials and Structures, Harbin Institute of Technology, Harbin 150080, P. R. China

[b] Key Laboratory of Microsystem and Microstructure of the Ministry of Education, Harbin Institute of Technology, Harbin 150080, P. R. China

* Corresponding author: Jiaqi Zhu

Email: zhujq@hit.edu.cn

Tel. / Fax: +86-451-86417970

Address: Post-box 3010, YiKuang Street 2, Harbin 150080 P.R. China

Abstract

The remarkable functional properties of diamond depend not only on its physical and chemical properties but also on its surface morphology. Ordered porous diamond with hierarchical structures is used in various applications in the fields of environment and energy management. However, obtaining such micro- and nanostructures via conventional techniques has proven to be challenging because of the superhardness and extreme chemical inertness of diamond. In this study, a strategy to create highly textured diamond films structured by vertical columnar crystals was developed. The mechanism of shape-evolution of diamond grains was proposed to account for the changes in the crystal shape from octahedron through cubo-octahedron to cube, followed by oxidation and hydrogenation. Shape evolution of diamond crystals during the initial fabrication stages was assessed by scanning electron microscopy, which

revealed that the surfaces of fabricated diamond consisted of rough octahedral {111} and smooth cubic {100} faces. The variation of the crystal shape depended on the relative growth rate of {111} faces to that of {100} faces during the growth process. Finally, highly ordered porous diamond films with switchable wettability properties were obtained by post-fabrication modification involving thermal etching in air followed by etching in hydrogen plasma.

1. Introduction

Diamond, one of the hardest substances in nature, is a functional material with extraordinary properties, such as high mechanical hardness, outstanding chemical inertness and high thermal conductivity [1-3]. Potential applications of diamond depend not only on its physical and chemical properties but also on its surface state and morphology [4,5]. The morphological structure of diamond makes morphological modifications feasible and hence, allows diamond to lend itself in broader applications. However, due to extremely high hardness and chemical inertness, it is not possible to modify diamond by mechanical processing or wet chemical etching. This is especially the case for the highly ordered diamond microstructures, which have been considered for use in fields of environment and energy management [6-8]. It is, therefore, important to develop a technically feasible and economically viable technique for fabricating synthetic diamond microstructures.

The nucleation and growth of heteroepitaxial diamond films have been the object of previous studies [9-11]. In particular, textured functional diamond films have recently attracted increasing attention with the primary focus placed on obtaining shape-controlled, ordered porous diamond films. Conventional scratching procedure, bias enhanced nucleation and seeding techniques have been employed in order to achieve improved heteroepitaxial growth of diamond nanocrystals [12-15].

Additionally, the effect of different gas mixtures, using multiple reacting gases (e.g., Ar, N_2, CO, CO_2 and H_2O), on diamond growth has been thoroughly investigated [16-18]. Diamond nanostructures with regular porosity have been synthesized using a bottom-up approach, for instance, the template-directed fabrication of 3D ordered macroporous diamond with the use of colloidal crystal templates, and the obtained diamond opal is a structurally perfect photonic crystal in the optical spectral region[19-21].

However, the shape control of micro- and nanostructured diamond films is limited by the templates used and the process complexity. Moreover, the templates must be selectively removed after crystal growth, which makes the synthesis method particularly challenging. The template method is based on the direct growth of diamond structures. This bottom-up strategy has the advantage of not requiring complex after-growth processing. However, the synthesis of ordered micro- and nanostructured diamond by selective area deposition is not a simple task, especially for achieving uniform growth on large substrates.

On the other hand, top-down processing of synthetic micro- and nanostructured diamond include catalytic, plasma-assisted reactive ion and thermal etching, which typically involve the use of reactive gases (e.g., argon, oxygen and hydrogen) or molten metal as etching agents and refractory metals or oxide materials as shadow masks [22]. However, during etching, the surface area of diamond crystals is strictly limited by the shadow masks used making complex hierarchical diamond configurations difficult to obtain. Therefore, the development of a suitable fabrication method for highly ordered diamond micro- and nanostructures is strongly needed.

In this study, the shape-evolution and shape-control of diamond grains were thoroughly investigated. The effect of the relative growth rate of the various crystal

planes on the evolution of the crystalline form from octahedron through cubo-octahedron to cube was assessed. The crystalline evolution was consistent with the specific surface energy of the constituent crystallographic diamond planes. Additionally, highly textured diamond films were fabricated by controlling the nucleation and the relative growth rate of the growing planes. The textured diamond films were treated by thermal etching in air and subsequent reactive ion etching in hydrogen plasma to obtain ordered porous diamond films. Detailed observations were made of the effect of operational conditions on the changes in morphology of the diamond grains. This helped understand the mechanisms of shape-evolution of ordered diamond micro- and nanocrystals.

2. Experimental

2.1. Materials

Silicon (100) wafers, 1.5 mm thick and 2 inches in size, (Aladdin Industrial Inc.), were used as substrates throughout all experiments. Diamond scratching was performed using diamond abrasion paste with a grain size of 1 μm (Best Diamond Industrial Co., Ltd.). An aqueous nanodiamond dispersion solution with nanodiamond particles in the range of 10-30 nm was supplied from ZhongNan Diamond Co., Ltd. Hydrofluoric acid, acetone, and ethanol were purchased from Beijing Chemical works Ltd. Deionized water was obtained from Harbin Baida Industrial Inc., and used throughout all experiments. Finally, N_2 (99.%), H_2 (99.999%), and CH_4 (99.999%) were purchased from Harbin Liming Co., Ltd.

2.2. Fabrication of ordered nanoporous diamond films

Initially, the silicon wafers were sequentially cleaned by acetone, ethanol, and deionized water to remove any organic impurities found on the surface, and dried by N_2. Then, the wafers were immersed in a 5 % solution of hydrofluoric acid for 3

minutes to remove the native oxide. The silicon wafers were subsequently coated with nanodiamond seeds through diamond scratching using the diamond abrasion paste, followed by spin-coating using the aqueous nanodiamond solution. An image of the aqueous nanodiamond solution and TEM images of the nanodiamond seeds are shown in Fig. S1. It was revealed that the aqueous nanodiamond solution did not precipitate and the nanodiamond seeds with sizes ranging from 10 to 30 nm were fully dispersed on the silicon wafer surface. Then, the nanodiamond seed-coated silicon wafer was put in a microwave-plasma-assisted chemical vapor deposition (MPACVD) system operating under vacuum. The substrate was directly heated by being immersed in plasma; no other heating source was used. The surface temperature of the sample was obtained using an infrared measuring system. A power of 3800 W and a ratio of 196/4 sccm for H_2/CH_4 at the temperature and pressure of 850 °C and 165 mbar, respectively, were used for diamond growth. The process parameters for the incubation and growth stages are shown in Table 1. Finally, the fabricated diamond films were treated by thermal etching in air followed by hydrogen atom etching in hydrogen plasma; process parameters are shown in Table 2 and Table 3.

2.3. Sample characterization

Surface morphology of specimens was examined by scanning electron microscopy (SEM, FEI Helios Nanolab 660i, operated at 5-20 kV). The morphology and microstructure of the samples were studied in detail by transmission electron microscope (TEM, FEI Tecnai G2 F30, operated at 300 kV). Raman spectra were acquired using a confocal Raman spectroscope (Horiba Jobin-Yvon Lab RAM HR800 System) with 458 nm laser excitation under ambient conditions. Water contact angles (WCA) were measured on an OCA20 system (Data-Physics) under ambient conditions; the volume of the water droplets was 5 μl. The WCA values reported

herein represent the average of measurements taken on five different areas of each sample. Finally, optical microscopy images were taken using a Nikon D7100 camera.

3. Results and discussion

To aid coalescence and produce smooth polycrystalline diamond films, a seeding step is usually required to reach the desired nucleation densities. In this paper, the impact of the scratching procedure and nanodiamond seeding techniques on nucleation densities and the corresponding variation of the diamond crystal shape were investigated. Fig. 1 shows the nucleation densities of nanodiamond clusters grown on silicon substrates seeded by the scratching procedure and nanodiamond seeding techniques. As shown in Fig. 1(a) and (b), nanodiamond clusters of various particle sizes grew mainly along the scratches. It was observed that the nucleation density on the substrate obtained by nanodiamond seeding was so high that it led to coalescence of the nanodiamond clusters, which nearly formed a thin film, as shown in Fig. 1(c). It was found that the nanodiamond seeding is a highly effective method for achieving high nucleation densities resulting in uniform growth of diamond films.

Fig. 2 shows the morphological features of diamond crystals grown on a substrate simultaneously seeded by the diamond scratching procedure and nanodiamond seeding technique (right part) after incubation for 10 minutes. The seeding method was a two step process: firstly, the Si substrate was coated with nanodiamond seeds through diamond scratching using the diamond abrasion paste and subsequent ultrasonic cleaning; secondly, a part of the substrate was quickly dipped into the aqueous nanodiamond solution and dried subsequently. The nanodiamond seeding technique gave rise to more diamond nucleation sites. This favored their subsequent coalescence and led to the growth of a uniform diamond film. In contrast, diamond growth on the substrate seeded by the diamond scratching procedure

involved the formation of diamond microspheres that they did not coalesce into a uniform film. As reported in our previous study, the diamond microspheres, obtained through diamond seeding, had porous aggregate structures and exhibited unique chemical properties [23]. Therefore, different diamond crystal shapes can be achieved by controlling the nucleation densities through different seeding techniques.

As reported by other workers, the relative growth rates in the [100] and [111] directions can also determine the crystal shape [24-26]. However, it is still urgently needed to give sufficient details about crystal shape evolution in order to depict the crystal growth mechanism. In this study, the shape evolution of diamond grains was thoroughly investigated. The effect of the relative growth rates on the change in the diamond crystal shape from rough octahedron through cubo-octahedron to cube was also assessed. The crystal shapes obtained are consistent with the specific surface energy of the respective growing planes, and they can be tailored to meet the requirements for different applications. As seen in Fig. 3(a), after incubation for 10 minutes, the diamond nuclei formed on the silicon substrate via the seeding technique led to the deposition of a diamond film with rough octahedral structures. The morphology of the diamond film varied with process time. As shown in Fig. 3(b)-(d), the crystal shape evolved from octahedron into cubo-octahedron after 60 minutes. The Fig. 3(d) shows that the triangular rough portions of the octahedral surface were composed of the {111} and {100} faces of diamond, while the smooth square portions were cubic {100} faces of diamond. The cubic {100} planes of diamond were formed on the top of the pyramid-like structures and were parallel to the silicon substrate.

Fig. 4 shows the schematic illustrations of the changes in crystal morphology as a function of the relative growth rate of constituent crystallographic planes. According

to a geometric model, the variation in the crystal shape from octahedron through cubo-octahedron to cube was determined by considering the growth ratio of {111} to {100} faces in their normal directions, and the model can be used as a guide to adjust the growth rates, times, and crystal orientation[27,28]. Similarly, the octahedron, cubo-octahedron and cube structures were determined by the ratio $R_{\{111\}}/R_{\{100\}}$ which was equal to $1/\sqrt{3}$, $2/\sqrt{3}$ and $\sqrt{3}$, respectively [29]. The corresponding schematic diagrams are shown in the Supplementary Information section (Fig. S2). Essentially, the growth ratio agrees with the specific surface energy of each growing plane based on the Gibbs-Curie-Wulff law [30]. The ratio of total surface energy to volume is the most important factor in determining the morphology during the nucleation stage. The lowest ratio corresponds to the octahedron structure, which is mainly composed of {111} crystallographic planes. Therefore, the initially formed diamond crystal shape was an octahedral thermodynamic equilibrium shape.

As shown in Fig. 4(a), the rough portions of the octahedral surface of fabricated diamond crystals were composed of {111} and {100} planes of diamond with the {111} planes being the dominant faces. A schematic illustration of the shape-evolution from rough octahedral to cubo-octahedral is depicted in Fig. 4(b), which shows the development of {100} planes on rough octahedral surfaces. As the ratios of $R_{\{111\}}/R_{\{100\}}$ ranged from $1/\sqrt{3}$ to $2/\sqrt{3}$, the {111} faces became significantly replaced by the constant growth of {100} faces, which were the preferential planes. As the growth process progressed, the rough octahedral structures evolved into smooth cube {100} faces of diamond. A schematic illustration of this evolution is shown in Fig. 4(c). The most favorable sites for deposition of active hydrocarbon radicals to form diamond crystals are steps, especially kinks or ledges. The rapid growth of the ledges or kinks will lead to the formation of flat {100} faces [31,32].

Fig. 4(d) is a schematic illustration showing the gradual development of {110} planes on the {111} faces during diamond grain growth. The {110} planes preferentially appeared at the edge of cubo-octahedral faces as the growth ratio of $R_{\{111\}}/R_{\{100\}}$ ranged from $2/\sqrt{3}$ to $\sqrt{3}$. The foregoing balance of the growth rates may be locally disrupted by the dominant growth of {110} planes. However, highly ordered columnar diamond crystals were fabricated under suitable growth conditions.

In this study, the diamond film composed of highly ordered columnar crystals was fabricated by using the aforementioned methods while varying the process parameters (Table 1) in order to control the crystal growth. As shown in Fig. 3(a), rough octahedral structures were formed during the incubation stage; the triangular rough portions of octahedral surfaces were composed of the dominant {111} faces and concomitant {100} faces. The appearance of {100} facets on the {111} faces was a good evidence of the presence of {100} planes on the rough {111} faces. As shown in Fig. 3(b)-(d), when the growth ratios of $R_{\{111\}}/R_{\{100\}}$ ranged from $1/\sqrt{3}$ to $\sqrt{3}$, the {111} faces were significantly reduced and the {100} faces became the preferential appearance. The cubic {100} faces, which appeared on the peaks of the octahedral structures, were very flat and smooth, while octahedral {111} faces were rough and irregular because of the interception of the two constituent crystallographic planes of {111} and {100}. As shown in Fig. 3(d), the {111} faces of diamond can be divided into {110} and {100} planes during the crystal growth procedure leading to the formation of cubic crystals as shown in Fig. 4(d).

In order to fabricate highly ordered porous diamond films composed of vertically aligned diamond nanocrystals, a simple method involving a two-step etching treatment was developed. As shown in the schematic in Fig. 5, the textured diamond film deposited by MPCVD was used as a placode: the first step of the heat treatment

which took place in air aimed to remove the diamond nanoparticles and non-diamond carbon impurities by oxidation, and the second step involved hydrogen atoms etching treatment in hydrogen plasma in order to fabricate highly ordered diamond nanocrystals. This two-step treatment enabled the formation of ordered, dense nanocrystals on the diamond surface without the aid of a mask or catalyst.

Fig. 6(a) shows the textured diamond film deposited after 60 minutes. The highly ordered textures seen in the SEM image suggest that the surface of the fabricated diamond film was due to the coalescence of vertically aligned columnar grains. The top of the columnar grains grew into cubic-smooth {100} planes of diamond which were parallel to the silicon substrate. The diamond nanoparticles and non-diamond carbon impurities lied between the diamond columnar grains in the diamond film.

The effect of the duration of the thermal treatment of fabricated textured diamond films on the removal of diamond nanoparticles and non-diamond type carbon impurities was investigated. As shown in Fig. 6(b), the textured diamond film was oxidized in air at 500 °C for 3 h. The carbon impurities found between the diamond columnar grains were removed, and diamond columnar arrays were subsequently formed, as shown in the magnified illustration of Fig. 6(b). In order to evaluate the effect of the oxidation temperature on the resulting diamond structure, the diamond film was exposed to air at 550 °C for the same times. As seen in Fig. 6(c), in the case of the diamond film thermally etched at 550 °C in air for 3 h, the diamond columnar grains were also sculptured, and the quadrate pillars evolved into tapered structures. So far, ordered fabricated diamond arrays are achieved via the oxygenation method; however, diamond films are intrinsically hydrophilic in the oxidized state. In order to investigate the special switchable wettability of porous

ordered diamond nanocrystals, the oxidized samples were subsequently etched in hydrogen plasma for 2 h. As shown in Fig. 6(d), the diamond arrays were transformed into nanoporous structures after etching in hydrogen plasma. The pores of the hydrogen-treated diamond film are larger than 3 nm and have a wide size distribution from 3 nm to 31nm as shown in Fig. S3. The results indicate highly ordered mesoporous structures. Additionally, the nanoporous diamond film was considered to be hydrogenated due to the long hydrogen plasma treatment. Hence, the hydrogenated nanoporous diamond film fabricated via oxidation and subsequent hydrogen plasma etching were expected to have special switchable wettability properties.

In order to investigate the effect of non-diamond carbon impurities on the water repellence of fabricated diamond films, the atomic structure of carbon in the test specimens was evaluated by Raman spectroscopy. Fig. 7 presents the Raman spectra corresponding to the treated diamond surfaces under the different etching steps shown in Fig. 7(a)-(d). From the Raman spectroscopy results, the peak at 1332 cm^{-1} is attributed to diamond, with no other carbon-related peaks present [33]. Based on the insets in Fig. 7 showing the Raman spectra between 1400 cm^{-1} and 1700 cm^{-1}, a substantial reduction in the graphite-like phase was confirmed based on the low intensity of the G-peak [34,35]. Hence, the hydrophobicity of the fabricated diamond films was not related to the presence of non-diamond carbon impurities in the films. Hydrophobicity was rather attributed to the hydrogenation of diamond films and their hierarchical structures.

It is to be noted that hydrogenated diamond is intrinsically hydrophobic. In the oxidized state, however, diamond becomes hydrophilic [36]. In order to investigate the effect of the surface structures on hydrophobicity, the test diamond specimens were kept hydrogenated. The diamond films oxidized in air were subsequently

hydrogenated via etching in hydrogen plasma for 5 minutes. Given that the etching time was short, the structure of the surface of diamond films was not significantly altered during the etching process in hydrogen plasma. The contact angles of fabricated hydrogenated diamond films with different structures are shown in Fig. S4. The wettability of hydrogenated samples under different treatment conditions is depicted in Fig. 8. It was found that the ordered diamond nanocrystals were highly hydrophobic having a contact angle of 138.5°. Hence, the hydrophobicity of thermally etched diamond films was superior to that previously reported for unmodified diamond films [5,37]. The hydrophobicity of diamond films increased with increasing surface roughness. Additionally, the water contact angle of oxidized diamond nanocrystals was smaller than 3° (Fig. S5). As shown in Fig. 8, the water contact angle ranged from 3°, for oxidized diamond film surfaces, to 138.5° for hydrogenated diamond films. Hence, synthetic diamond films with switchable wettability were fabricated.

4. Conclusions

Highly ordered polycrystalline diamond films have been fabricated via a two-step process including orientated seed growth during the incubation stage followed by ordered diamond film growth. The shape-evolution of diamond grains was responsible for the changes in the crystal shape from octahedron through cubo-octahedron to cube. The appearance of {100} facets on {111} faces was a strong evidence for the presence of {100} planes on the rough {111} faces. The rough portions of the octahedral surfaces were composed of {111} and {100} planes of diamond. The division of the {111} faces of diamond into {110} planes and {100} planes explained the appearance of cube crystals along with cubo-octahedral crystals during the growth stage. Therefore, it is crucial to control the growth conditions in

order to obtain highly textured diamond films. Textured, highly ordered diamond films were modified into nanoporous films via thermal etching in air and subsequent reactive ion etching in hydrogen plasma. The hydrogenated diamond nanocrystals exhibited extreme water repellence with a contact angle of 138.5°. However, in the oxidized state, the diamond surfaces became hydrophilic, and the contact angle was lower than 3°. Hence, highly ordered nanoporous diamond films with switchable wettability can be fabricated, which increases the potential for use in various applications.

Acknowledgement

The financial support from the National Science Fund for Distinguished Young Scholars (Grant No. 51625201), the National Natural Science Foundation of China (Grant No.51372053), the Project supported by the Foundation for Innovative Research Groups of the National Natural Science Foundation of China (Grant No. 11421091), the Major State Basic Search Program (No.2014CB46505), the National Natural Science Foundation of China (Grant No. 51702066), the National Key Research and Development Program of China (2016YFE0201600), and the International Science & Technology Cooperation Program of China (2015DFR50300) is acknowledged. Qiang Wang and Jie Bai contributed equally to this work.

References

[1] Yang Y, Li H, Cheng S, Zou G, Wang C, Lin, Q. Robust diamond meshes with unique wettability properties. Chem. Commun. 2014; 50(22): 2900-4.

[2] Kaner R B, Gilman J J, Tolbert S H. Designing superhard materials. Science 2005, 308(5726): 1268-2.

[3] Graebner J E, Jin S, Kammlott G W, Herb J A, Gardinier C F. Large anisotropic thermal conductivity in synthetic diamond films. Nature 1992; 359(6394): 401-3.

[4] Babinec T M, Hausmann B J, Khan M, Zhang Y, Maze J R, Hemmer P R, et al. A diamond nanowire single-photon source. Nature Nanotech. 2010; 5(3): 195-5.

[5] Ostrovskaya L Y, Ral'chenko V G, Vlasov I I, Khomich A A, Bol'shakov A P. Hydrophobic diamond films.Prot. Met. Phys. Chem. Surf. 2013; 49(3): 325-7.

[6] Kondo T, Kodama Y, Ikezoe S, Yajima K, Aikawa T, Yuasa M. Porous boron-doped diamond electrodes fabricated via two-step thermal treatment. Carbon 2014; 77: 783-7.

[7] Wei M, Terashima C, Lv M, Fujishima A, Gu Z Z. Boron-doped diamond nanograss array for electrochemical sensors.Chem. Commun. 2009; (24): 3624-3.

[8] He Y, Lin H, Wang X, Huang W, Chen R, Li H. A hydrophobic three-dimensionally networked boron-doped diamond electrode towards electrochemical oxidation. Chem. Commun. 2016; 52(51): 8026-4.

[9] Schreck M, Roll H, Stritzker B. Diamond/Ir/SrTiO 3: a material combination for improved heteroepitaxial diamond films. Appl. Phys. Lett. 1999; 74(5): 650-3.

[10] Klein O, Mayr M, Fischer M, Gsell S, Schreck M. Propagation and annihilation of threading dislocations during off-axis growth of heteroepitaxial diamond films. Diamond Relat. Mater. 2016; 65: 53-6.

[11] Tang Y H, Golding B. Stress engineering of high-quality single crystal diamond by heteroepitaxial lateral overgrowth. Appl. Phys. Lett. 2016; 108(5): 052101.

[12] Mandal S, Thomas E L, Jenny T A, Williams O A. Chemical nucleation of diamond films. ACS Appl. Mat. Interfaces 2016; 8(39): 26220-6.

[13] Wolter S D, Stoner B R, Glass J T, Ellis P J, Buhaenko D S, Jenkins C E, et al. Textured growth of diamond on silicon via in situ carburization and bias-enhanced nucleation. Appl. Phys. Lett. 1993; 62(11): 1215-3.

[14] Williams O A, Douhéret O, Daenen M, Haenen K, Ōsawa E, Takahashi M. Enhanced diamond nucleation on monodispersed nanocrystalline diamond. Chem. Phys. Lett. 2007; 445(4): 255-4.

[15] Arnault J C, Demuynck L, Speisser C, Le Normand F. Mechanisms of CVD diamond nucleation and growth on mechanically scratched Si (100) surfaces. Eur. Phys. J., B Cond. Matter Phys. 1999; 11(2): 327-7.

[16] Dunst S, Sternschulte H, Schreck M. Growth rate enhancement by nitrogen in diamond chemical vapor deposition—a catalytic effect. Appl. Phys. Lett. 2009; 94(22): 224101.

[17] Choi I H, Weisbecker P, Barrat S, Bauer-Grosse E. Growth of highly oriented diamond films by the MPCVD technique using CO-H_2, CH_4-H_2 and CH_4-N_2-H_2 gas mixtures. Diamond Relat. Mater. 2004; 13(4): 574-7.

[18] Tallaire A, Rond C, Bénédic F, Brinza O, Achard J, Silva F, Gicquel A. Effect of argon addition on the growth of thick single crystal diamond by high-power plasma CVD. Phys. status solidi A 2011; 208(9): 2028-5.

[19] Zakhidov AA, Baughman RH, Iqbal Z, Cui C, Khayrullin I, Dantas SO, Marti J, Ralchenko VG, Carbon structures with three-dimensional periodicity at optical wavelengths. Science 1998, 282: 897-5.

[20] Kurdyukov DA, Feoktistov NA, Nashchekin AV, Zadiranov YM, Aleksenskii AE, Vul AY, Golubev VG, Ordered porous diamond films fabricated by colloidal crystal templating. Nanotechnology 2011, 23: 015601.

[21] Sovyk DN, Ralchenko VG, Kurdyukov DA, Grudinkin SA, Golubev VG, Khomich AA, Konov VI, Photonic crystals of diamond spheres with the opal structure. Phys. Solid State 2013, 55: 1120-4.

[22] Masuda H, Watanabe M, Yasui K, Tryk D, Rao T, Fujishima A. Fabrication of a nanostructured diamond honeycomb film. Adv Mater 2000;12(6):444–7.

[23] Wang Q, Bai J, Dai B, Yang Z, Guo S, Yang L, et al. Robust superhydrophobic diamond microspheres for no-loss transport of corrosive liquid microdroplets. Chem. Commun. 2017; 53(15): 2355-4.

[24] Zolotukhin AA, Dolganov MA, Alekseev AM, Obraztsov AN, Single-crystal diamond microneedles shaped at growth stage. Diam. Relat. Mater. 2014; 42: 15-6.

[25] Silva F, Achard J, Brinza O, Bonnin X, Hassouni K, Anthonis A, De Cort K, Barjon J, High quality, large surface area, homoepitaxial MPACVD diamond growth. Diam. Relat. Mater. 2009; 18(5): 683-15.

[26] Harada Y, Hishinuma R, Terashima C, Uetsuka H, Nakata K, Kondo T, Yuasa M, Fujishima A, Rapid growth of diamond and its morphology by in-liquid plasma CVD. Diam. Relat. Mater. 2016, 63, 12-5.

[27] Bogatskiy A, Butler JE, A geometric model of growth for cubic crystals: Diamond. Diam. Relat. Mater. 2015; 53: 58-8.

[28] Delfaure C, Tranchant N, Mazellier JP, Ponard P, Saada S, Monitoring texture formation during diamond growth by specular and diffuse reflectance interferometry. Diam. Relat. Mater. 2016; 69: 214-7.

[29] Silva F, Achard J, Brinza O, Bonnin X, Hassouni K, Anthonis A, et al. High quality, large surface area, homoepitaxial MPACVD diamond growth. Diam. Relat. Mater. 2009; 18(5): 683-15.

[30] Markov I V. Crystal growth for beginners: fundamentals of nucleation, crystal growth and epitaxy[M]. World scientific, 2016.

[31] Spear K E, Frenklach M. Mechanisms for CVD diamond growth[M]. John Wiley & Sons, Inc, 1994.

[32] Huang D, Frenklach M. Energetics of surface reactions on (100) diamond plane. J. Phys. Chem. 1992; 96(4): 1868-8.

[33] Knight D S, White W B. Characterization of diamond films by Raman spectroscopy. J. Mater. Res. 1989; 4(2): 385-393.

[34] Ferrari A C, Meyer J C, Scardaci V, Casiraghi C, Lazzeri M, Mauri F, et al. Raman spectrum of graphene and graphene layers. Phys. Rev. Lett. 2006; 97(18): 187401.

[35] Chhowalla M, Ferrari A C, Robertson J, Amaratunga G A J. Evolution of sp^2 bonding with deposition temperature in tetrahedral amorphous carbon studied by Raman spectroscopy. Appl. Phys. Lett. 2000; 76(11): 1419-3.

[36] Pinzari F, Ascarelli P, Cappelli E, Mattei G, Giorgi R. Wettability of HF-CVD diamond films. Diamond Relat. Mater. 2001; 10(3): 781-5.

[37] Zhou Y B, Yang Y, Liu W M, Ye Q, He B, Zou Y S, et al. Preparation of superhydrophobic nanodiamond and cubic boron nitride films. Appl. Phys. Lett. 2010, 97(13): 133110.

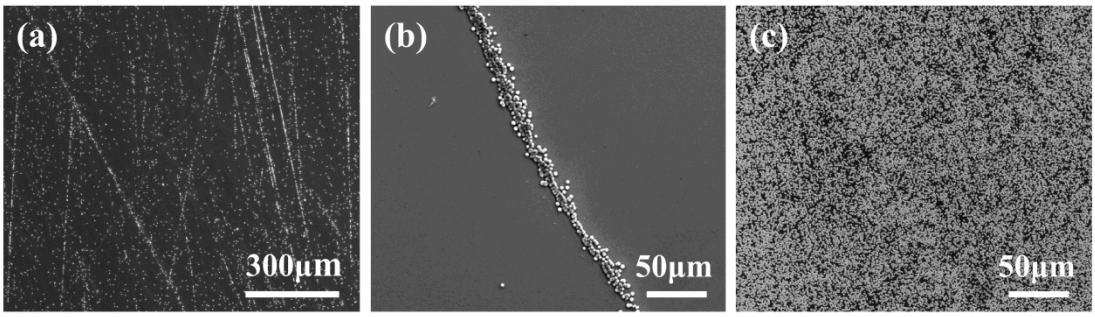

Fig. 1 SEM micrographs of diamond nucleation densities on silicon substrates seeded by different techniques: (a) silicon substrate seeded by the diamond scratching procedure, (b) magnified SEM image of a typical scratch, (c) silicon substrate seeded by the nanodiamond seeding technique.

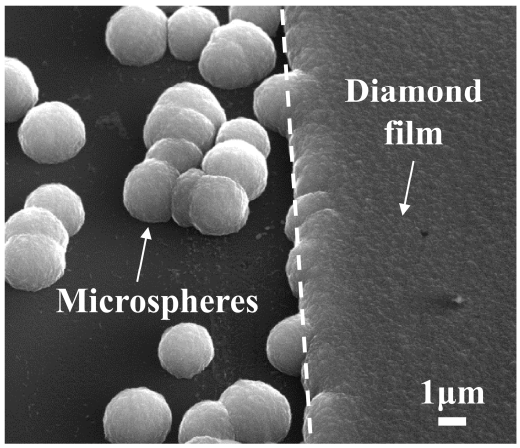

Fig. 2 SEM image of diamond crystals deposited after incubation for 10 minutes. Silicon substrate was simultaneously seeded by the diamond scratching procedure (on the left) and nanodiamond seeding technique resulting in the growth of a diamond film (on the right).

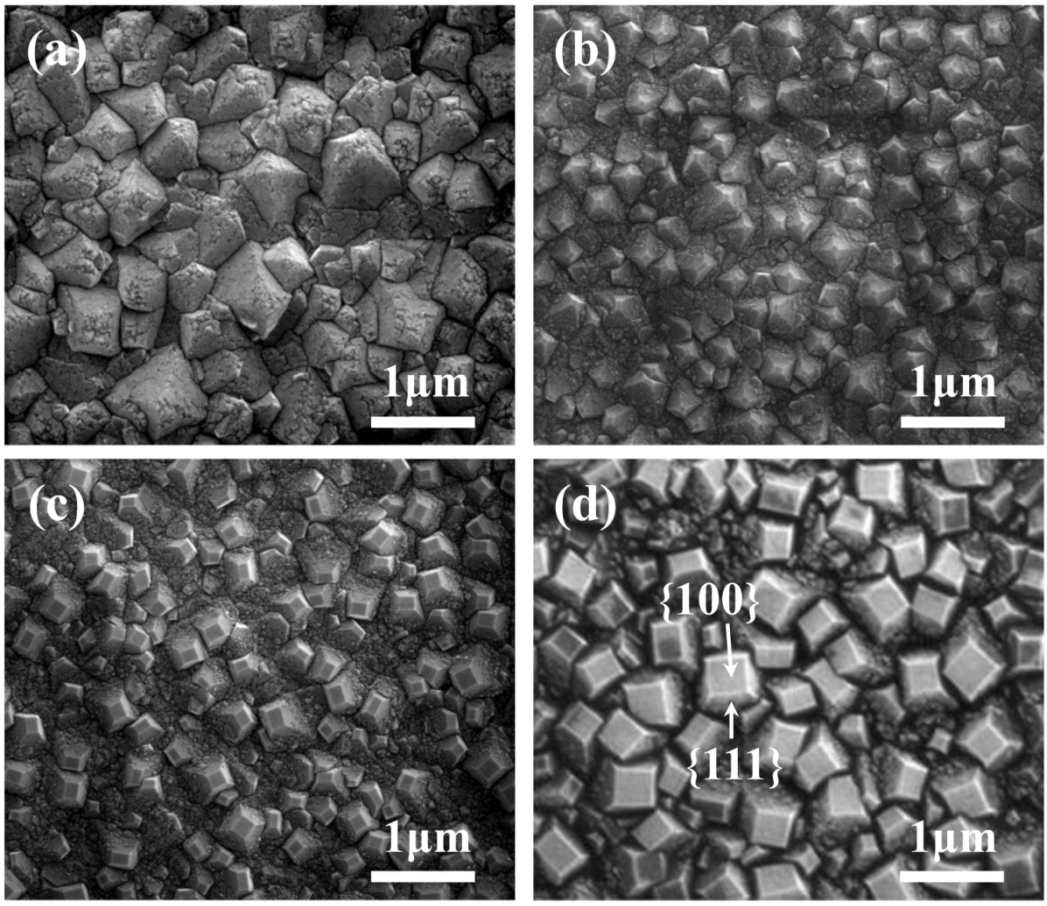

Fig. 3 SEM images of the diamond crystal morphology obtained under the same deposition conditions for different growth times: (a) 10 minutes, (b) 20 minutes, (c) 30 minutes and (d) 60 minutes.

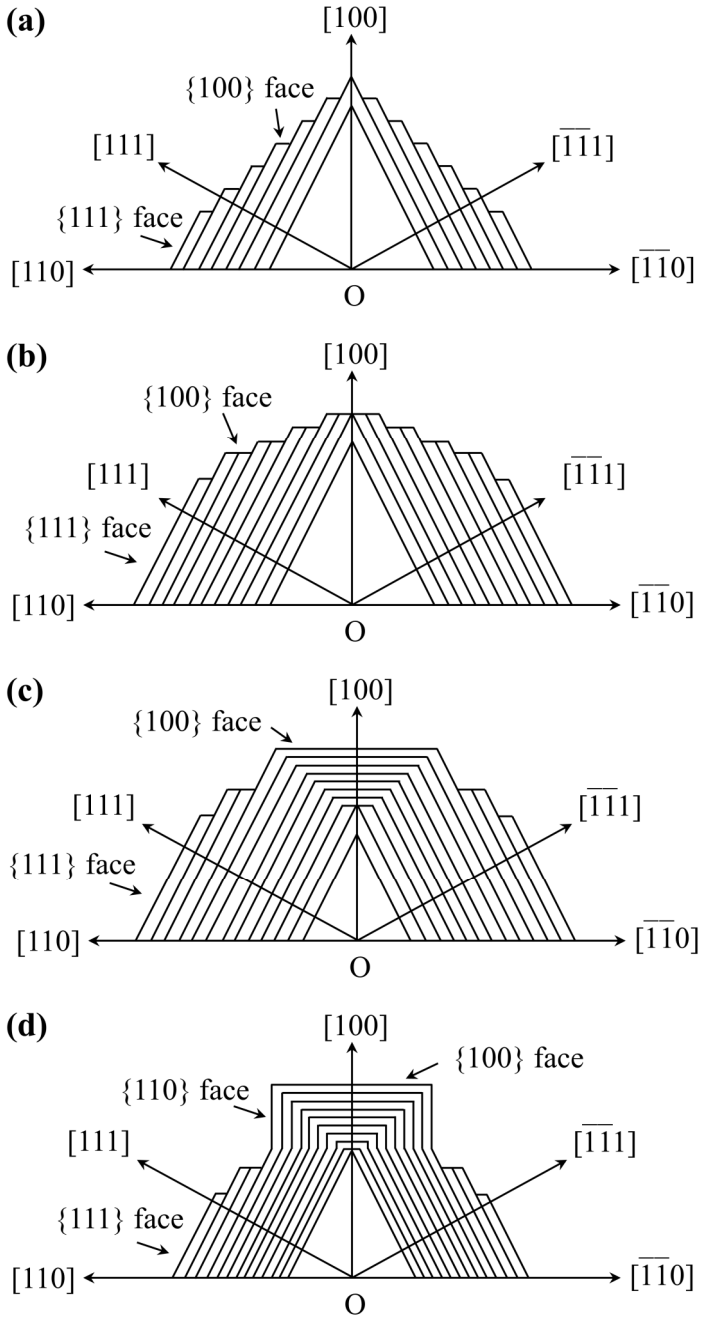

Fig. 4 Schematic illustration of the changes in crystal morphology with the relative growth rate of constituent crystallographic planes: (a) a part of rough octahedral diamond grain, (b) the shape-evolution of diamond crystals from octahedral to cubo-octahedral configurations, (c) the crystal shape with rough {111} and smooth-cubic {100} faces and (d) the gradual development of {110} planes on the {111} faces during diamond grain growth.

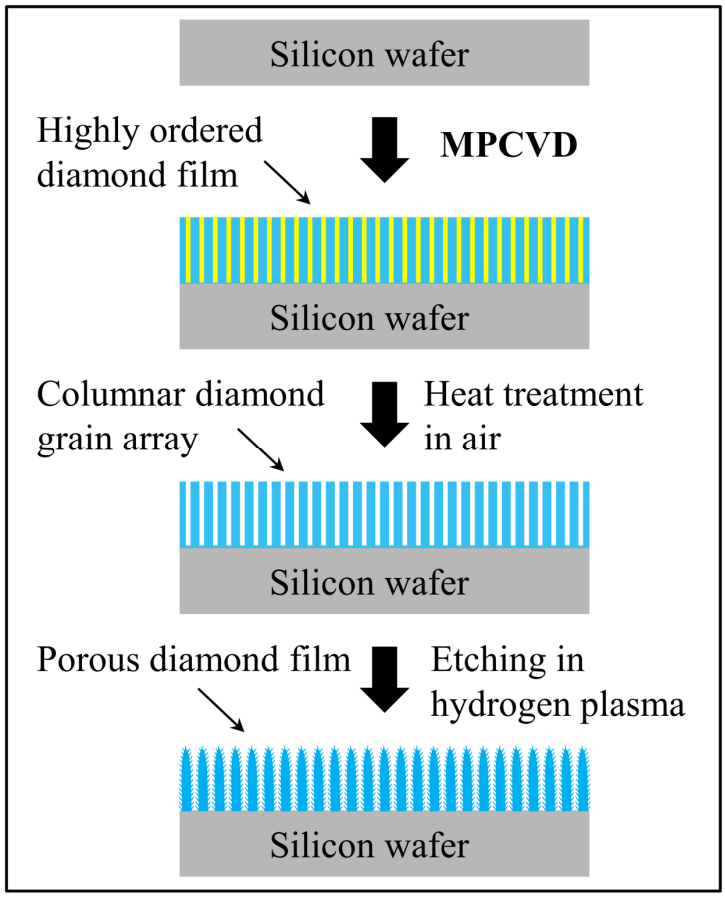

Fig. 5 Schematic illustration of the fabrication process for porous diamond films via thermal etching in air and subsequent reactive ion etching in hydrogen plasma. The final film consists of highly ordered diamond nanocrystals.

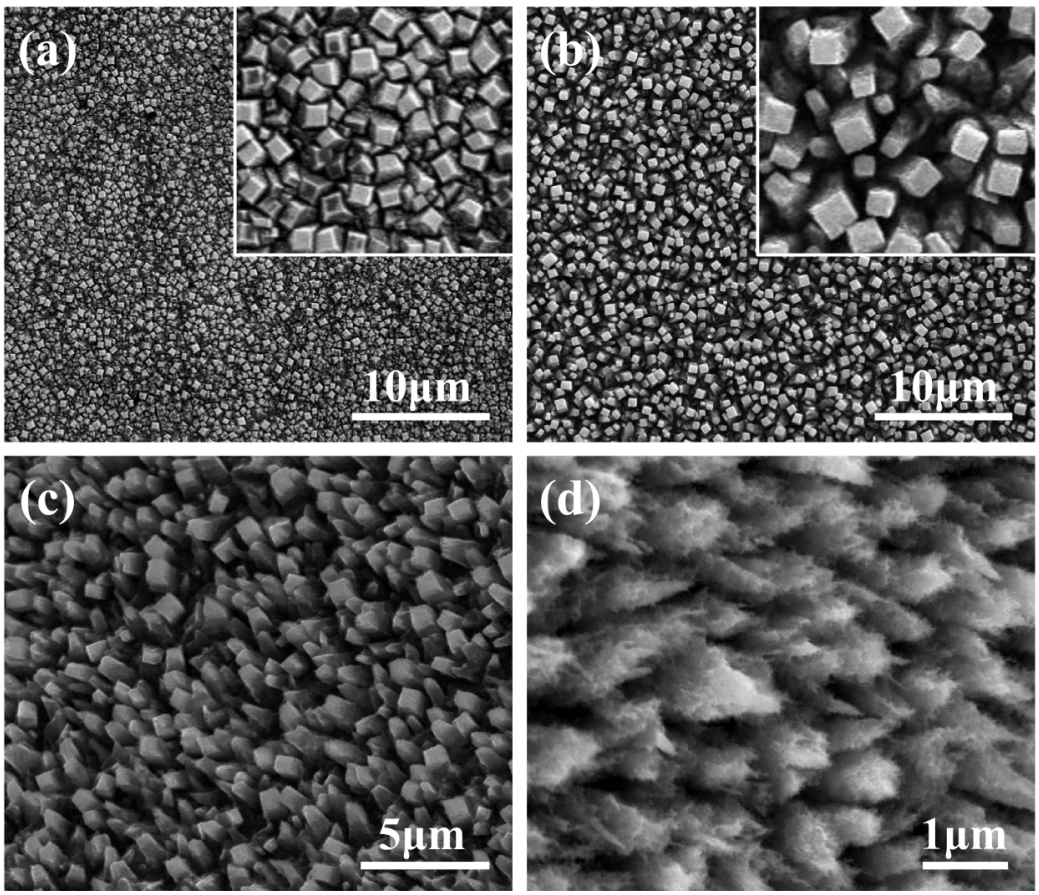

Fig. 6 SEM images of the textured diamond film after etching under different etching conditions: (a) as-fabricated diamond film, (b) diamond film thermally etched at 500 °C in air for 3 h, (c) diamond film thermally etched at 550 °C in air for 3 h, (d) diamond film modified via reactive ion etching at 600 °C in hydrogen plasma for 2 h.

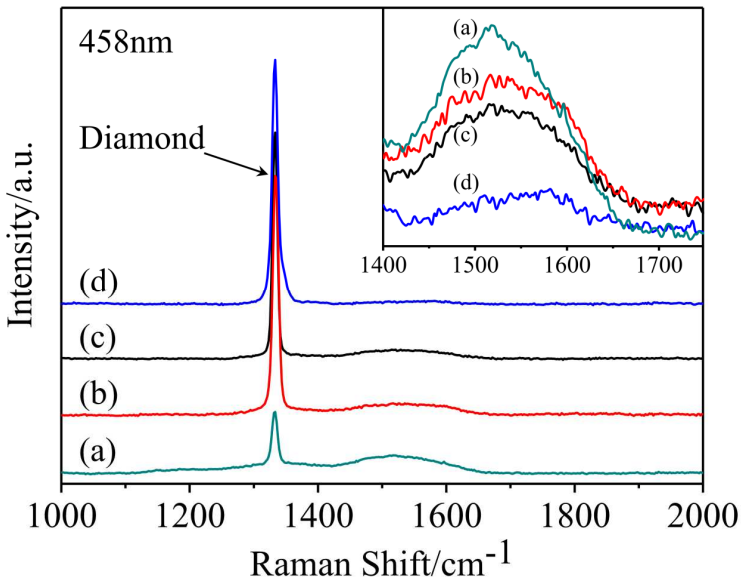

Fig. 7 Raman spectra of untreated and treated synthetic diamond surfaces. (a) as-fabricated diamond film, (b) diamond film thermally etched at 500 °C in air for 3 h, (c) diamond film thermally etched at 550 °C in air for 3 h and (d) diamond film etched at 600 °C in hydrogen plasma for 2 h.

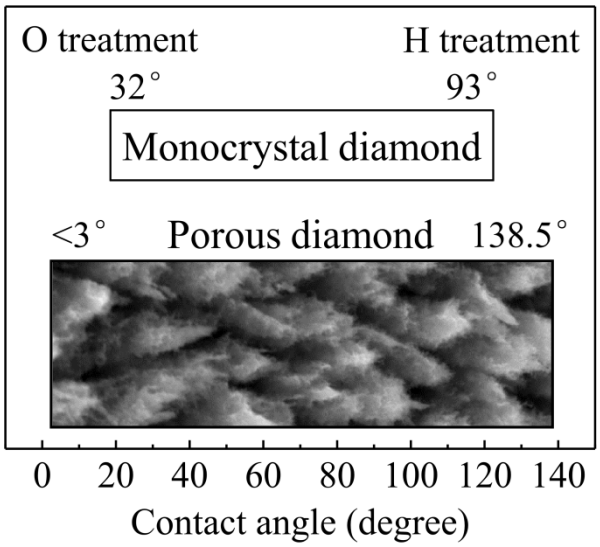

Fig. 8 The water contact angle range for single diamond crystals and porous diamond films. Low and high values correspond to diamond surfaces modified via oxidation and hydrogenation, respectively.

Table 1 Process parameters for the deposition of textured diamond films on silica substrates during the incubation and growth stages.

Parameter	Incubation stage	Growth stage
Microwave power (W)	3800	3800
Total flow (sccm)	200	200
H_2 flow (sccm)	188	196
CH_4 flow (sccm)	12	4
Pressure (mbar)	195	165
Temperature (°C)	1000	850
Duration (min)	10	10-60

Table 2 Etching process parameters for the fabrication of diamond films.

Parameter	Step 1 (in air)	Step 2 (in air)	Step 3 (in H plasma)
Temperature (°C)	500	550	600
Duration (min)	180	180	120

Table 3 Process parameters of H plasma treatment

Parameter	
Microwave power (W)	2000
H_2 flow (sccm)	200
Pressure (mbar)	120
Temperature (°C)	600
Time (min)	120